Mechanism of Ubiquinol Oxidation by the bc1 Complex: Role of the Iron Sulfur Protein and Its Mobility†

ARTICLE *in* BIOCHEMISTRY · NOVEMBER 1999

Impact Factor: 3.02 · DOI: 10.1021/bi990961u · Source: PubMed

6 AUTHORS, INCLUDING:

Antony R Crofts
University of Illinois, Urbana-Champaign
248 PUBLICATIONS **11,370** CITATIONS
SEE PROFILE

Li-shar Huang
State University of New York Upstate Medical…
51 PUBLICATIONS **2,204** CITATIONS
SEE PROFILE

Zhaolei Zhang
University of Toronto
118 PUBLICATIONS **4,485** CITATIONS
SEE PROFILE

Edward A Berry
State University of New York Upstate Medical…
72 PUBLICATIONS **4,030** CITATIONS
SEE PROFILE

Mechanism of Ubiquinol Oxidation by the bc_1 Complex: Role of the Iron Sulfur Protein and Its Mobility†

Antony R. Crofts,*,‡ Mariana Guergova-Kuras,‡ LiShar Huang,§ Richard Kuras,‡ Zhaolei Zhang,§ and Edward A. Berry*,§

Center for Biophysics and Computational Biology, University of Illinois at Urbana−Champaign, Urbana, Illinois 61801, and Lawrence Berkeley National Laboratory, University of California, Berkeley, California 94720

Received April 27, 1999; Revised Manuscript Received August 16, 1999

ABSTRACT: Native structures of ubihydroquinone:cytochrome *c* oxidoreductase (bc_1 complex) from different sources, and structures with inhibitors in place, show a 16−22 Å displacement of the [2Fe-2S] cluster and the position of the C-terminal extrinsic domain of the iron sulfur protein. None of the structures shows a static configuration that would allow catalysis of all partial reactions of quinol oxidation. We have suggested that the different conformations reflect a movement of the subunit necessary for catalysis. The displacement from an interface with cytochrome c_1 in native crystals to an interface with cytochrome *b* is induced by stigmatellin or 5-*n*-undecyl-6-hydroxy-4,7-dioxobenzothiazole (UHDBT) and involves ligand formation between His-161 of the [2Fe-2S] binding cluster and the inhibitor. The movement is a rotational displacement, so that the same conserved docking surface on the iron sulfur protein interacts with cytochrome c_1 and with cytochrome *b*. The mobile extrinsic domain retains essentially the same tertiary structure, and the anchoring N-terminal tail remains in the same position. The movement occurs through an extension of a helical segment in the short linking span. We report details of the protein structure for the two main configurations in the chicken heart mitochondrial complex and discuss insights into mechanism provided by the structures and by mutant strains in which the docking at the cytochrome *b* interface is impaired. The movement of the iron sulfur protein represents a novel mechanism of electron transfer, in which a tethered mobile head allows electron transfer through a distance without the entropic loss from free diffusion.

The ubihydroquinone:cytochrome *c* oxidoreductase (bc_1 complex)[1] (E.C. 1.10.2.2) and the related b_6f complex of oxygenic photosynthesis are central components of the major electron-transfer chains that carry the energy flux of the biosphere. The bc_1 complex of the mitochondrial respiratory chain transfers electrons from ubihydroquinone (quinol) to cytochrome (cyt) *c* in the aqueous phase and catalyzes the coupled transfer of protons across the membrane. Our understanding of the function of these enzymes at the atomic level has been greatly aided by structures recently solved by X-ray crystallography. These include cyt *f* (the equivalent of cyt c_1 in the b_6f complex) from chloroplasts (*1*, *2*) and the Rieske iron sulfur protein (ISP) from the beef heart mitochondrial complex (*3*) and chloroplasts (*4*), all crystallized as water-soluble fragments generated by proteolysis or mutagenesis. A partial structure of the beef heart mitochondrial complex at ∼2.9 Å resolution has been published by Xia and colleagues (*5*, *6*). However, the crystals were disordered in the region of the ISP and cytochrome c_1, and this precluded a detailed consideration of the mechanistic role of these subunits. More complete structures for the complexes from chicken, rabbit, and beef heart mitochondria have been provided by Zhang et al. (*7*) and Iwata et al. (*8*). Kim et al. (*9*) have recently reported further refinement of the Xia et al. (*6*) crystals, with and without inhibitors, including density for the ISP fitted by use of the soluble fragment (*3*).

Although the mitochondrial bc_1 complexes contain 10−11 subunits, the catalytic functions are served by a core consisting of three subunits, cyt *b*, cyt c_1, and the ISP. A

† We acknowledge with gratitude the support for this research provided by NIH Grants GM 35438 (to A.R.C.) and DK 44842 (to E.A.B.), and by the Office of Health and Environmental Research, U.S. Department of Energy, under Contract DE-AC03-76SF00098 (E.A.B.).

* Corresponding authors: for functional aspects, A.R.C., Center for Biophysics and Computational Biology, University of Illinois at Urbana−Champaign, 388 Morrill Hall, 505 S. Goodwin, Urbana, IL 61801; for structural aspects, E.A.B., Structural Biology Division, Lawrence Berkeley National Laboratory, 250 Melvyn Calvin Lab 5230, University of California, Berkeley, CA 94720-5230.

‡ University of Illinois.

§ University of California.

[1] Abbreviations: bc_1 complex, ubihydroquinone:cytochrome *c* (or c_2) oxidoreductase; b_H, higher potential cytochrome *b* heme; b_L, lower potential cytochrome *b* heme; cyt, cytochrome; DCCD, dicyclohexylcarbodiimide; EPR, electron paramagnetic resonance; [2Fe-2S], iron sulfur cluster of the Rieske-type iron sulfur protein; ISP, Rieske-type iron sulfur protein; ISP^{ox} and ISP^{red}, oxidized and reduced states of the iron sulfur protein; ISP_B or ISP_C, iron sulfur protein with the mobile extrinsic domain docked at cytochrome *b* or cytochrome c_1 interface, respectively; LH1, light-harvesting complex 1 of bacterial photosynthesis; MOA-, β-methoxyacrylate, or similar group, acting as the pharmacophore of a class of inhibitors acting at the Q_o site; QH_2, ubihydroquinone or quinol; Q, ubiquinone or quinone; Q_i site, quinone reducing site; Q_o site, quinol oxidizing site; Q_{os} and Q_{ow}, postulated strongly and weakly binding quinone molecules bound to the quinol oxidizing site; -PEWY-, highly conserved span with this sequence in single-letter amino acid code; UHDBT, 5-*n*-undecyl-6-hydroxy-4,7-dioxobenzothiazole.

10.1021/bi990961u CCC: $18.00
Published on Web 11/05/1999

similar enzyme in photosynthetic and respiratory species from the α-division of the purple bacteria catalyzes the same reaction with cyt c_2 as acceptor. The complex in purple bacteria contains only three or four subunits, the three core subunits and sometimes a fourth of unknown function. This catalytic core has been highly conserved across the bacterial−mitochondrial divide.

The bc_1 complex functions through a modified Q cycle (*10*−*13*), which explains with economy the main features of the activity. Quinol is oxidized at the Q_o site of the complex. The reaction is rate-determining and has a relatively high activation barrier (*14*). Quinol oxidation occurs in a bifurcated reaction, in which one electron is transferred to a high-potential chain and the other to a low-potential chain. The high-potential chain, consisting of the ISP, cyt c_1, and cyt *c* (or c_2), transfers one electron from quinol to an acceptor (cytochrome oxidase in mitochondria, the oxidized photochemical reaction center in photosynthetic systems). It is generally supposed that this leaves a semiquinone at the Q_o site, but this has not been detected. Because the semiquinone formed is unstable, the reaction at the Q_o site appears to be a concerted electron transfer to the high- and low-potential chains. The low potential chain consists of two cyt *b* hemes (cyt b_L and cyt b_H, for low- and high-potential hemes), which serve as a pathway through which electrons are transferred across the coupling membrane from semiquinone at the Q_o site to the Q_i site, at which quinone is reduced to quinol. To provide the two electrons at the Q_i site required for reduction of quinone, the Q_o site oxidizes 2 equiv of quinol in successive turnovers. The first electron at the Q_i site generates a relatively stable semiquinone that is reduced to quinol by the second electron.

Interpretations of reaction kinetics have in the past assumed a solid-state model of the protein structure, in which redox centers were fixed spatially. A more dynamic picture of the mechanism of electron transfer between the Q_o site and cyt c_1 has emerged from the structures for mitochondrial complexes (*6*−*9*). These showed that the extrinsic C-terminal domain (the head) of the ISP is not fixed but is found in different positions in different crystals, close to catalytic interfaces on either cyt c_1 or cyt *b*. In the structure of Xia et al. (*6*), the [2Fe-2S] center was close to a myxothiazole binding site (identified as the Q_o site) but was too distant from heme c_1 to allow rapid electron transfer. The authors therefore speculated that the distance could be bridged by protein chains between the two centers or by a major conformational change between oxidized and reduced forms of the ISP. In the native structures of the chicken, rabbit, and beef complexes reported by Zhang et al. (*7*) the [2Fe-2S] center was closer to cyt c_1 by ∼16−22 Å than in the native structure of Xia et al. (*6*). In crystals of the chicken complex with stigmatellin in place (*7*), the ISP had moved from the position in native crystals close to cyt c_1 to bring the [2Fe-2S] center to a position similar to that in the crystals of Xia et al. (*6*). In the stigmatellin-containing crystals, the distance to cyt c_1 was also too great for rapid electron transfer, but it was clear, since the structure was well-resolved, that no protein chains spanned the distance. In the native structures, the ISP was close enough to cyt c_1 for rapid electron transfer but was separated from the Q_o site by a cleft, which would prevent interaction with the substrate at the site. Since none of these static configurations could function in all the partial reactions of quinol oxidation, we suggested that a movement of the ISP head between reaction interfaces with cyt *b* and cyt c_1 was essential for catalysis (*7*, *15*), as summarized in Figure 1. The evidence from earlier work for a relatively loose association of the ISP with the complex could possibly reflect the relatively loose binding indicated by this motility (*16*−*21*).

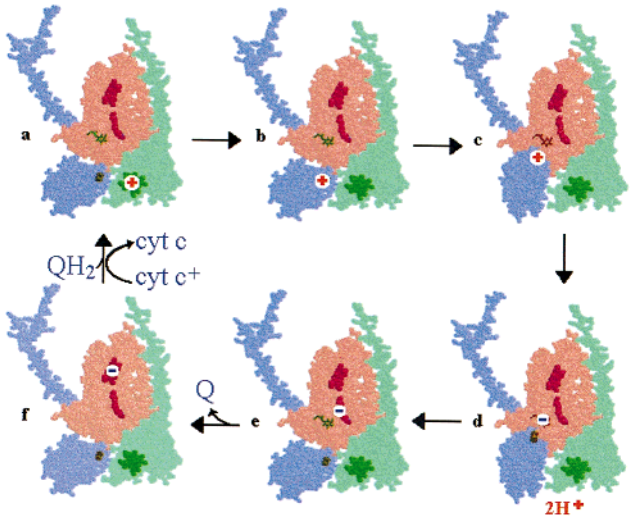

FIGURE 1: Scheme showing the movement of the ISP involved in quinol oxidation at the Q_o site. The complex is represented by the three catalytic subunits (cyt *b*, red; cyt c_1, green; ISP, blue), shown as transparent space-filling models, revealing the metal centers. The arrival of an oxidizing equivalent on cyt c_1 is shown by the ringed + in panel a, which is transferred to the ISP (in the ISP_C position) in panel b. The oxidation of QH_2 (a−c) is indicated by the appearance of an electron (ringed −) at the Q_o site, indicating formation of a semiquinone in panel d (in panels c and d, ISP is in the ISP_B position), and its transfer to the *b*-cytochrome chain (e, f), leaving quinone (e), which leaves the site (f). Note that the electron transfer from QH_2 to the [2Fe-2S] center to form the semiquinone anion releases $2H^+$ to the aqueous phase (d), balancing the charges in the transition (c − d).When the reduced form undergoes oxidation (a − b), the ISP subunit must be associated with cyt c_1, to allow for the rapid electron transfer observed. This configuration (ISP_C) is the position observed in the Zhang/Berry native structures.After formation of the oxidized form, the subunit must move to the docking interface on cytochrome *b*, close to the Q_o site, before reduction by the quinol can occur (c − d). This configuration (ISP_B) is that observed in the stigmatellin-containing structure (*7*) and corresponds to the [2Fe-2S] position seen in the structure of Xia et al. After reduction by electron transfer from QH_2, the subunit must move back to its association with cyt c_1 (to the ISP_C configuration) (d − e) in order that reoxidation can initiate the next turnover of the Q_o site. The oxidation of quinol must be completed by electron transfer from the semiquinone to the Q_i site, and exchange of Q at the Q_o site for QH_2 (e − a).

In this paper, we examine structural aspects of the movement of the ISP in greater detail. We report on the structure of the interfaces and the changes that occur when stigmatellin binds and induces the change in configuration of the ISP. We discuss information about mechanism that can be gleaned from strains generated by specific mutagenesis at residues that contribute to the interfaces. The modifications of Q_o site properties in many of these mutants support the hypothesis that docking of the ISP at the interface on cyt *b* is essential for function. We note other examples of tethered redox centers and discuss the mechanistic advantages of this novel mechanism of electron transfer. A more complete account of the structure of the chicken heart mitochondrial complex (*7*) and preliminary reports of some

Table 1

data set name[a]	cell parameters			resolution, redundancy, completeness, precision				in shell 3.5−3.6 Å[c]		temperature factor[d]			
	a	*b*	*c*	d_{min}	measurements	unique reflections (completeness)	R_{sym}[b] (I > 3σ)	$\langle F/\sigma_F \rangle$	completeness ($F > \sigma_F$)	*B* overall	*B*11	*B*22	*B*33
1BCC	169.582	182.521	240.577	3.16	556 456	123 869 (0.916)	0.102	9.6	0.99	25.9	83.5	17.3	17.5
3BCC	173.178	179.727	238.220	3.20	394 429	111 849 (0.910)	0.243	2.9	0.93	33.0	57.9	29.3	25.1
2BCC	173.464	182.448	241.328	3.00	306 685	117 928 (0.771)	0.131	4.0	0.76	20.4	35.9	14.4	20.0
MYX	173.177	181.217	240.003	3.40	365 806	90 815 (0.871)	0.228	3.3	0.89	22.2	59.0	13.4	14.4
MOA	171.838	181.925	240.412	3.59	159 573	70 736 (0.741)	0.203		0.00	29.7	59.0	31.2	22.3

[a] The data set 1BCC is from a crystal with no inhibitors, and 3BCC is from one with antimycin and stigmatellin. 2BCC, MYX, and MOA are from crystals with stigmatellin, myxothiazole, and MOA-stilbene, respectively. [b] In calculating R_{sym}, reflections with negative measured intensity were not rejected unless the absolute value was greater than 3σ. Therefore, the R_{sym} value is very high in the highest-resolution shells, where the intensity of most reflections is below the noise level, and should not be compared with R_{sym} values calculated after excluding weak rejections. The French and Wilson method (*24*), as implemented in the CCP4 program *truncate*, was used to estimate maximum likelihood values of *F* and σ_F from all reflections including those with negative intensity. Only reflections with $F > 2\sigma_F$ were used in refinement. [c] Average F/σ_F and completeness were calculated in a narrow shell around 3.5 Å (shell slightly different for each data set). *F* was calculated from *I* by the *truncate* method (see Materials and Methods). Completeness was calculated by excluding those reflections for which $F < \sigma_F$. [d] The isotropic overall *B*-factor was estimated by scaling each data set against structure factors calculated from the model of the native bc1 complex (1bcc) in which all atomic *B*-factors were set to 20 to avoid low-resolution information from the solvent/protein contrast (solvent was absent in the model). The relative *B*-factor obtained was added to 20 to give the *B*-factor for the crystal. Anisotropic temperature factors *B*11, *B*22, and *B*33 were determined by scaling the raw data set against F_{calc} as described above but with anisotropic scaling.

mechanistic aspects of this work (*7, 15*) have appeared elsewhere. In separate papers, we discuss physicochemical aspects of the movement of the ISP (*22*) and the reactions at the Q_o site in which bound quinol is oxidized after formation of a reaction complex with the oxidized ISP docked on cyt *b* (*23*).

MATERIALS AND METHODS

Crystallographic Methods. Crystallographic aspects of structural determination of the complexes were discussed at length in an earlier paper (*7*). Structural coordinates of the refined native chicken heart mitochondrial bc_1 complex and of the complex with stigmatellin, or stigmatellin and antimycin, are available as files 1bcc, 2bcc, and 3bcc, respectively, from the Brookhaven Protein Data Bank. All residue numbering in this paper is according to the sequence assigned in file 1bcc.

Refinement data for these structures and for three new structures discussed in this and companion papers are given in Table 1. The internal order of the crystals, as manifested in resolution limit and temperature factor, is a major limitation to the interpretation of the data presented here. To use as much as possible of the valid diffraction data without introducing noise from reflections too weak to be measured, we used a combined cutoff based on both resolution and intensity. The resolution cutoff was in most cases set considerably higher than the effective resolution of the crystal, to make use of the few strong reflections in the last shells that could be measured with significance. Then during model refinement only reflections with $F > 2\sigma_F$ were used, resulting in very low completeness for the last shells but retaining what significant information there was. Since application of a σ cutoff during averaging of symmetry-related reflections results in major overestimation of weak reflections, a cutoff of -3σ was used at that stage (default cutoff of the software used, *Scalepack*). Subsequently the French and Wilson method (*24*), as implemented in the CCP4 program *truncate*, was used to estimate maximum likelihood values for *F* from all reflections including those with negative intensity. Only at this stage were weak reflections rejected, with only reflections with $F > 2\sigma_F$ used during model refinement. This resulted in very low completeness for the last shells but retained what significant information was there. The resolution cutoff is thus a poor indicator of quality of the data set, as it does not take into account incompleteness of the high-resolution shells. A better indicator is the total number of unique reflections used. To make this parameter independent of the space group and put it in more intuitive units, it can be expressed as the "effective resolution", defined as the resolution of a complete data set having the same number of unique reflections (*25*). This parameter is presented in Table 2, column 4. As an indicator of the relative amount of high-resolution data available from the different crystals, we have presented in Table 1 the mean F/σ_F and completeness for each data set in a narrow resolution shell around 3.5 Å.

Preparation of Images. Structural figures were prepared by use of the Netscape plug-in, Chime (MDL Information Systems, Inc., San Leandro, CA, version 2.0.3). Although the mitochondrial bc_1 complex has been described as a dimer (*5*−*9*), a functional monomer is represented in many of the figures, unless the dimeric context is required. It should be noted that this functional monomer differs from the crystallographic monomer, since the extrinsic domain (the head) of the ISP of one monomer interacts with catalytic interfaces of cyt *b* and cyt c_1 of the other monomer. Stereo figures are for crossed-eye viewing. Surfaces of residues or protein were calculated by use of the Chime 2.0 surface function, with a mesh spacing of 0.45 Å, and the default probe size of 1.4 Å.

Secondary Structural Analysis. Profiles for hydropathy, amphipathy, and conservation moment, and helical wheels and cylinders to display the results graphically, were calculated with routines from the pSAAM package of programs (26; A. R. Crofts, unpublished results). For calculation of conservation, the information gain was calculated at each residue in an alignment of sequences. For the ISP, six mitochondrial sequences (including two vertebrate, two fungal, and two plant ISPs), and four bacterial sequences were used. For cyt *b*, 16 sequences were used, including 13 mitochondrial (three fungal, seven vertebrate, and three plant) and three bacterial cytochromes *b*. The

Table 2

	data refinement											
data set name[a]	D_{min} (refine)	reflns used ($F_o > 2\sigma F_o$)	D_{min}[b] (effective)	no. of atoms in model	data to parameters ratio[c]	*R*-free value	coordinate error[d]	$\langle B_{atomic} \rangle$ for cyt *b*	Q_i site occupant	$\langle B_{atomic} \rangle$ for Q_i occupant	Q_o site occupant	$\langle B_{atomic} \rangle$ for Q_o occupant
1BCC*	3.16	107 167	3.35	31 444	1.70 (0.85)	0.310	0.56	65.6	U10	81		
1BCC	3.16	121 980	3.21	31 444	1.94 (0.97)	0.322	0.69	48.7	U10	71		
3BCC*	3.5	71 026	3.85	31 530	1.13 (0.56)	0.321	0.56	46.	AMY[e]	37	STG	37
3BCC	3.2	104 521	3.38	31 530	1.66 (0.83)	0.323	0.91	46.7	AMY	37	STG	28
2BCC	3.0	115 822	3.30	31 514	1.84 (0.92)	0.297	0.61	44.4	U10	62	STG	28
MYX	3.40	88 208	3.60	31 510	1.40 (0.70)	0.315	0.73	40.8	U10	64	MYX	15
MOA	3.59	68 462	3.92	31 488	1.09 (0.54)	0.321	0.71	39.65	U10	75	MOS	18.48

[a] Names are as described in Table 1. The asterisk on 1BCC and 3BCC indicates the original refinement of these data sets used for the coordinates submitted in spring 1998 and released July 1998. [b] Effective resolution is a resolution such that a complete data set with the same cell parameters and extending to that resolution would have the same number of reflections as the number of reflections in the data set in question greater than 2 times the σ level (*25*). [c] The data to parameters ratio is calculated as the ratio of reflections to 4 times the number of atoms in a monomer or dimer. The factor of 4 is because *x*, *y*, and *z* coordiantes and *B*-factor are refined for each atom. Because we used noncrystallographic constraints to link atoms in different monomers, the number of atoms in a monomer is more appropriate. [d] Coordinate error is the ESD from cross-validated SigmaA treatment over the same resolution range and with the same bulk solvent correction as used in refinement. [e] AMY, antimycin.

resulting profiles for information gain were used to generate a Rasmol/Chime script to color the protein, using a scale changing from red (completely conserved), through yellow and green, to blue (unconserved).

RESULTS AND DISCUSSION

Positions of the Fe Centers. The positions of the ISP iron centers in four different structures are shown in Figure 2, top. The orientation of the iron sulfur protein for the ISP docked at cyt *b* in the stigmatellin-containing structure is shown by a cartoon of the protein backbone. For the three other structures, only the protein within 8.0 Å is shown. It is apparent that the [2Fe-2S] centers are significantly displaced in the different crystal forms. Zhang et al. (*7*) were able to identify the ISP in chicken, rabbit, and beef heart complexes, in a configuration similar to that of the proteolytic fragment of Iwata et al. (*3*), which was used for initial orientation. Iwata et al. (*3*) noted from their earlier crystallographic studies that the ISP is a particularly well-ordered structure, with a system of internal H-bonds, disulfide links, and salt bridges locking the liganding loops into a fixed configuration. However, in the beef mitochondrial $P6_5$ crystal from Iwata et al. (*8*) an additional position of the ISP head, with a somewhat different conformation, has been found. Although the ISP protein was not resolved in the original structure of Xia et al. (*6*), Kim et al. (*9*) have more recently reported that the structure could be located, by using the soluble fragment of Iwata et al. (*3*) in a rigid body search around the [2Fe-2S] center. Better defined structures were found for crystals with UHDBT and stigmatellin, with the ISP in a position similar to that previously shown in the stigmatellin structure of Zhang et al. (*7*).

Distances from Reaction Partners. In all our native structures, the [2Fe-2S] center was close to cyt c_1, as summarized by Zhang et al. (*7*). In Figure 2 (top), the distances between the nearest Fe of the [2Fe-2S] center and the Fe of the cyt c_1 heme are shown for three of our structures. In the beef hexagonal crystals (position 1) ($P6_5$-22), the distances found are 15.8 Å from atom Fe2 (liganded by His-161) of the [2Fe-2S] center to the Fe of heme c_1 (as shown), ~7.6 Å from Fe2 to the nearest atom of the heme propionate, or ~3.4 Å from Nϵ2 of His-161 to O1δ of the heme propionate. This latter distance is close enough for a H-bond. For the chicken complex in the presence of stigmatellin the Fe-to-Fe distance for the same Fe pair is 32.6 Å (as shown by position 4), similar to that in the native structure Xia et al. (*6*). For the native chicken complex, the equivalent Fe-to-Fe distance was 20.4 Å (position 2). From the distance dependence of rates of electron transfer (*23, 24*), it can readily be calculated that the distances in the native configuration of Zhang et al. (*7*), but not that of Xia et al. (*6*), could allow a rapid electron transfer to cyt c_1. We suggest that the closest distance, seen in our beef $P6_522$ crystals, was likely to be the configuration from which reaction occurred, with the differences between positions in the various native complexes representing alternative positions from which the close approach needed for electron transfer could readily be attained. Iwata et al. (*8*) have shown a configuration in their $P6_522$ crystals, solved at about 3.0 Å resolution, similar to that in the $P6_522$ crystals, Zhang et al. (*7*) and they also considered this the likely reaction configuration. They have also identified an alternative position in one monomer of the $P6_5$ crystals, also included in Figure 2 (as position 3, taken from PDB file 1bgy; *8*) for comparison.

Although the configuration close to cyt c_1 would be suitable for electron transfer from ISP to cyt c_1, it is unlikely that it would also be effective for the electron transfer from quinol to ISP, because the subunit is not properly configured for the reaction with this other partner. The distance from the [2Fe-2S] center to the expected position of the substrate (taken as the center of the H-bonded stigmatellin ring in crystals containing the inhibitor, or the center of a quinone modeled in the distal position) is ~22 Å. Although this is in principle close enough for rapid electron transfer in a suitable protein matrix, and there are protein contacts between the ISP and cyt *b*, the [2Fe-2S] center is separated from the Q_o site by a distinct cleft, which is almost certainly aqueous. There is compelling evidence from EPR spectroscopy that inhibitors which bind at the Q_o site interact closely with the [2Fe-2S] center (*27*−*32*) and evidence that both quinone and quinol also interact (*33*−*36*). This cleft, and the separation between the center and the binding site, are therefore unexpected and suggest that this static conformation cannot represent the form in which interactions of the ISP with substrate and inhibitors at the Q_o site occur. In the native structure, Xia et al. (*6*) and the stigmatellin-containing

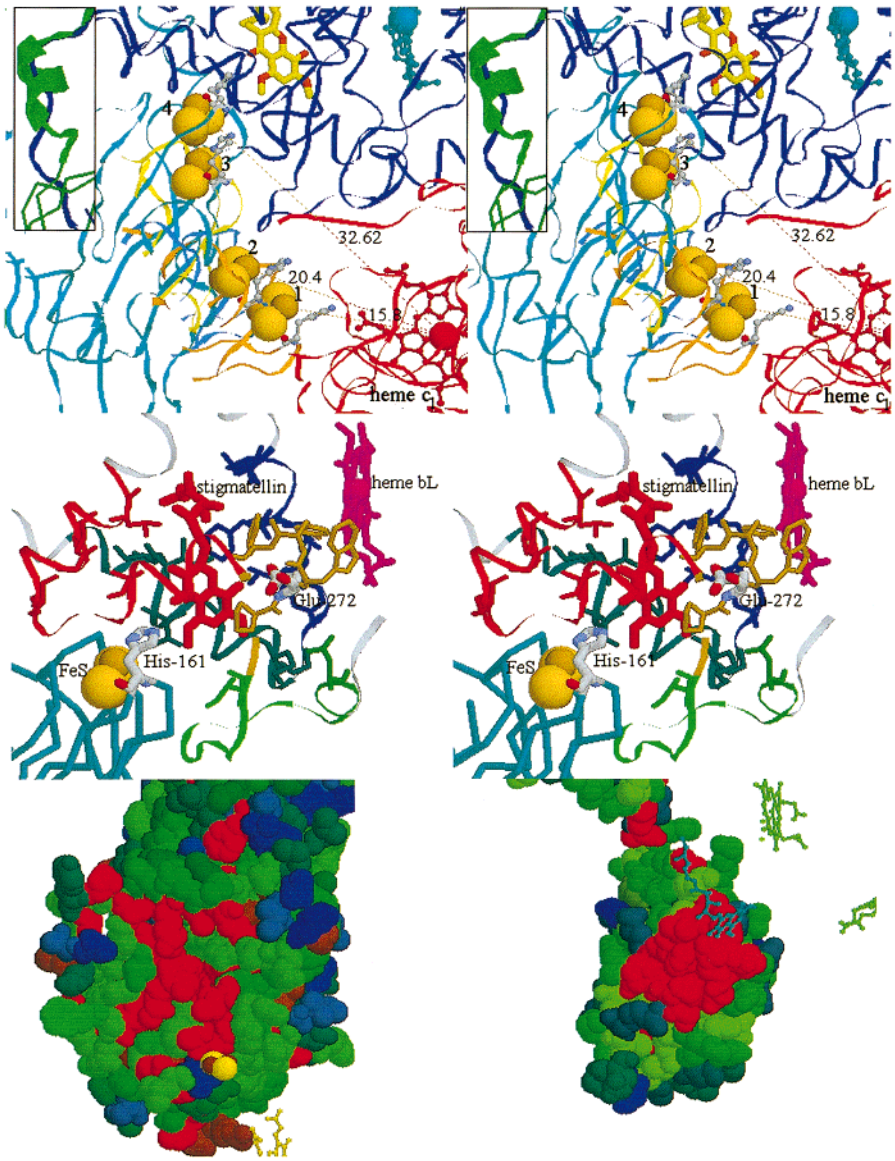

FIGURE 2: Different positions of the ISP and the conservation of the docking interface. (Top) Ribbon diagrams showing the configuration of the [2Fe-2S]-binding domain of the ISP in different crystal forms. The cyt *b* (dark blue) and cyt c_1 (red) subunits are shown with the prosthetic groups as ball-and-stick models. Heme b_L is in cyan, and heme c_1 is in red. The ISP in the stigmatellin-induced position in the chicken complex is shown as a pale blue ribbon, with the cluster indicated by 4. For the other positions of the ISP, only protein within 8.0 Å of the cluster is shown, for clarity. The cluster domain in the native position in the beef hexagonal complex ($P6_522$ crystals) (numbered 1) is shown with a protein ribbon; the domain in chicken native crystals (numbered 2) is shown in pale green; the cluster domain in the int position in $P6_5$ crystals (*8*) is shown in yellow and numbered 3. In each position, His-161 is also shown as an indicator of orientation. The values against the lines connecting centers show the distances in angstroms between them. Distances were estimated from the nearest iron of the [2Fe-2S] center to the Fe of heme c_1. The inset shows the hinge region from a different perspective, with the structure between residues 63 and 73 as a Richardson cartoon to show the extension through which the movement occurs. The green helix is the native configuration, and the blue extended chain is the stigmatellin-induced configuration. Coordinates are from PDB files 1bcc and 2bcc. (This panel is presented as a stereopair for crossed-eye viewing.) (Middle) The Q_o site, showing the docking of the ISP at the cyt *b* interface. The spans contributing to the Q_o site are shown as ribbons colored as follows: C-terminal end of C helix (blue), cd1 helix (green-blue), ef loop (green), -PEWY- (yellow), ef helix (orange), and N-terminal end of F helix (red). Residues at which mutation induces resistance to inhibitors are shown as stick models. The ISP is shown as a backbone model, with the [2Fe-2S] center as a CPK-colored space-filling model. His-161 is shown as a ball and stick model in CPK colors. (This panel is presented as a stereopair.) (Bottom) Space-filling models of cyt *b* (left) and the ISP (right) oriented to show the docking interfaces. Residues are colored according to the degree of conservation (see Materials and Methods).

structure of Zhang et al. similar distances (31−32 Å) are seen between the iron sulfur cluster of the ISP and cyt c_1 heme. However, in the structure of Zhang et al., the protein is quite well resolved. A density connection between the inhibitor and the ISP is apparent in the electron density maps, which we have modeled as an H-bond between Nϵ of His-161 of ISP and carbonyl and methoxy oxygens of the ring system of the inhibitor (see Figure 2, middle). The structure therefore demonstrates the interaction of the subunit with the inhibitor at the Q_o site previously predicted from biophysical studies (*27*−*32*). The configuration close to cyt *b* provides a model for the reaction complex and likely represents the configuration of the ISP in which electron transfer from QH_2 at the Q_o site to the [2Fe-2S] occurs.

Since neither structure seems fitted to the full dynamics of function as assayed by kinetic experiments, we have

suggested that the difference between crystals must reflect a conformational change of the complex involving movement of the head of the ISP, which is necessary for catalysis (*7*, *15*; see Figure 1).

Structural aspects: the interface between cyt b and ISP. Figure 2 (top) shows four configurations of the ISP with respect to the other catalytic subunits. The location of the Q_o site is indicated in the middle panel of Figure 2 by stigmatellin. In the native structure the site is vacant. The position of the ISP in our myxothiazole or MOA-stilbene-containing crystals (*23*) is the same as in the native structure (*7*, *15*, *23*). Figure 2 (middle) shows an overview of the Q_o site in which the spans contributing to the structure have been color-coded. The side chains indicate the sites at which mutation leads to inhibitor resistance or functional modification. The figure shows the protein with stigmatellin in place and the ISP docked at the interface with cyt *b*, and with His-161 of the ISP (also a ligand to the [2Fe-2S] cluster) and Glu-272 of cyt *b* providing ligands to stigmatellin.

A number of features of interest to an understanding of the mechanism of the Q_o site should be noted. Spans contributing to the site include the C-terminal end of the transmembrane helix C (blue in Figure 2, middle), the cd1 helix (green-blue), the ef loop, including a coil from the end of the helix E (green), the -PEWY- turn (yellow), the small ef helix (orange) connecting the -PEWY- turn to transmembrane helix F, and the N-terminal end of helix F (red). These contributions had been predicted from model building based on sequence analysis and the sites at which inhibitor-resistant lesions had been identified or at which changes in function had been generated by specific mutagenesis (*26*, *35*−*37*).

(a) The spans define two features: (i) a volume that represents the quinol binding pocket and (ii) a concave surface that forms the interface at which the ISP docks in the stigmatellin-containing crystals. The binding pocket is somewhat buried and is located between the position of the [2Fe-2S] center and the heme of cyt b_L. The extra electron density in crystals containing stigmatellin is located in this binding pocket (Figure 2, top and middle). The binding pocket is bifurcated, with a lobe proximal to cyt b_L and a distal lobe that opens to the ISP docking interface. Stigmatellin binds with its ring system in the distal lobe, and myxothiazole or MOA-type inhibitors bind with the pharmacophore in the proximal lobe (*6*−*9*, *23*). We discuss the implications of this bifurcated binding pocket in detail in a separate paper (*23*).

(b) In Figure 2 (top), the positions of the ISP cluster numbered 1 (beef $P6_522$) and 2 (chicken) are from native crystals. Note the substantial gap between the [2Fe-2S] center and the quinol-binding pocket and the distant position of the [2Fe-2S] center. There is some contact between the ISP head and the ef loop cyt *b*, involving (in ISP) conserved residues Lys-94, Leu-142, and Gly-143 (the latter two close to the [2Fe-2S] center) and residues Pro-262, Leu-263, Thr-265, and Val-264 (in cyt *b*). Distances appropriate for H-bonds are found between Nζ of Lys-94 (ISP) and O of Pro-262 (cyt *b*), and between backbone O of Leu-142 and -NH of Thr-265. These interactions may constrain the ISP in the ISP_C configuration or guide its diffusion. Cluster position 3 (Figure 2, top) is taken from the intermediate position found in one monomer from $P6_5$ crystals of the beef complex (*8*).

(c) The model in Figure 2 (middle) and the protein and the cluster position 4 (top) are from the structure in the presence of stigmatellin. Although the extrinsic ISP domain was initially located by fitting the structure of Iwata et al. (*3*) to the electron density, the structure of this domain shows some changes due to refinement. However, no major differences from that of the water-soluble fragment are apparent, and the structure did not differ dramatically for the ISP in its different positions. Stigmatellin was modeled to occupy the electron density due to stigmatellin in the crystals. A contact to the ISP seen in the density has been modeled as a H-bond between Nϵ H-161 of the ISP (one of the [2Fe-2S] ligands) and carbonyl and methoxy oxygens of the stigmatellin ring. A similar H-bonding was suggested previously to account for the effects of stigmatellin on the EPR spectrum and E_m value of the ISP (*3*, *38*, *39*). A second ligand is provided by Glu-272 of cyt *b*, which points into the pocket to form a H-bond from Oϵ1 to the OH of the ring of stigmatellin. This configuration of the side chain is rotated ∼120° compared to the native, myxothiazole, or MOA-stilbene structures. We discuss the possible role of this residue in release of the second proton in a companion paper (*23*).

Residues contributing to the interfacial surfaces on all three subunits are substantially conserved (Figure 2, bottom), even though they are exposed to the aqueous phase in one or other of the configurations shown; the same face of the ISP is involved in both docking configurations. The high degree of conservation suggests that the interfacial structures fit a specific purpose, as would be expected from an involvement in the docking necessary to the mechanism proposed.

Structural changes at the interface on cyt b when stigmatellin binds and the ISP docks. Differences between the native and stigmatellin-containing structures show that in addition to the movement of the ISP, the Q_o site undergoes a significant conformational change on binding stigmatellin [compare Figure 3, panels A (native), and B (with stigmatellin)]. The main effect is an enlargement of the volume to accommodate the inhibitor. This expansion of the site involves a substantial displacement of the -PEWY- loop in one direction, and of the cd1 helix in the opposite direction, to widen the volume by ∼2 Å. More modest displacements of the C, ef, and F helices also occur. At the ISP interface, the enlargement of the site leads to a substantial movement of Ile-269 and neighboring structure. Within the pocket, several side chains rotate to accommodate the two rings of the stigmatellin head. The hydrophobic tail extends into the lipid phase through a tunnel, which we presume to be the entry and exit channel.

Several significant new H-bonds are formed at the docking interface. Most dramatically, His-161 of the ISP forms a contact with stigmatellin, modeled as a pair of H-bonds to carbonyl and O-methyl oxygens of the inhibitor. At the interface, Lys-288 rotates so that the NH_2 group reaches the OH of Ser-152, which rotates to meet it. This rotation of lysine stops it from interfering with the ISP docking and also positions it so as to H-bond to backbone O atoms of ISP His-141 (a cluster ligand) and Thr-140. Ser-152 is not conserved among bacterial cyt *b* sequences, and the mutation of Gly to Ser in *Rhodobacter capsulatus* did not modify function (*36*), so this interaction is not essential. Access of the ISP to the inhibitor is provided by an opening between

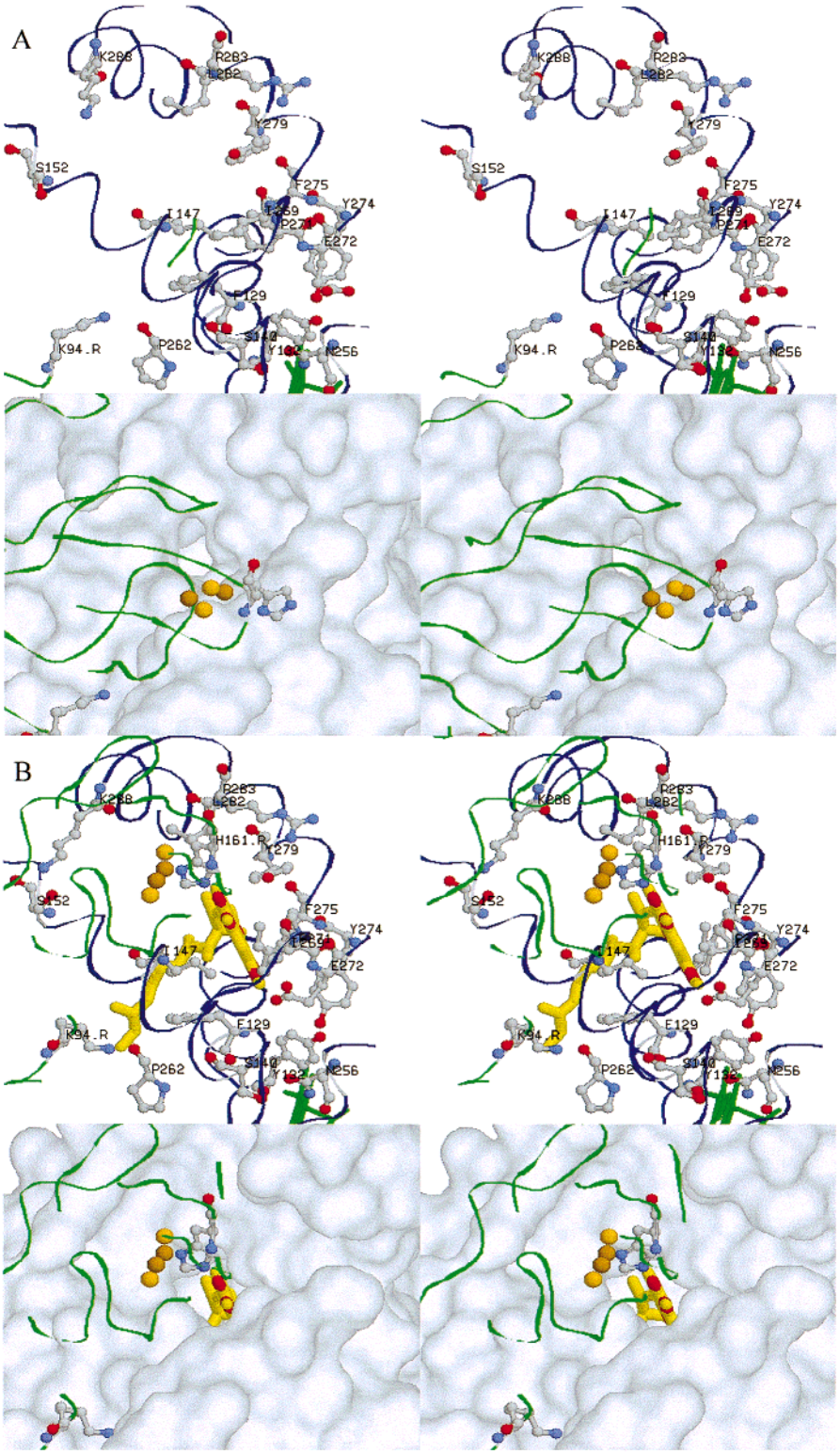

FIGURE 3: Interfacial surface on cytochrome *b* at which the ISP docks. (A) (Top) Residues at the interfacial surface in the native configuration. The structure has been cut away to show the residues discussed. (Bottom) Surface of the protein, showing the topography and the narrowed orifice into the Q_o-binding site. The position of the ISP is indicated by the cluster (CPK-colored small spheres) and His-161, with the protein represented by a green ribbon. (B) (Top) Residues at the interfacial surface in the stigmatellin-induced configuration. (Bottom) Surface, showing the orifice through which His-161 gains access to stigmatellin. Stigmatellin is shown as a green stick model with O atoms in red. The ISP is shown as in panel A. The structure of the ISP has been cut away so as not to obscure the view. All panels are presented as stereopairs for crossed-eye viewing.

the inhibitor binding pocket and the docking interface. On binding stigmatellin, Tyr-279 rotates so that the OH can form a H-bond with NH1 of Arg-283. It also H-bonds to backbone O of Cys-160, one element of a conserved cystine bridge in the ISP. This rotation facilitates access to the inhibitor, which is also aided by the widening on displacement of the -PEWY- loop. Changes deeper in the pocket, including the rotation of Glu-272 into the pocket noted above, are discussed in a

separate paper (*23*). Impaired function upon site-directed mutagenesis of several of these residues has demonstrated their importance to function. One contact of interest is maintained between the native and stigmatellin structures—the H-bond between Nζ of Lys-94 (ISP) and O of Pro-262 (cyt *b*) (Figure 3). This appears to provide a pivot for the rotation.

The dramatic movement of the ISP between positions in the absence and presence of stigmatellin seen in Figures 1−3 is accomplished by a rotation of the head about an axis passing through the ISP near residues 92 and 182. The movement of the ISP from its docking interface on cyt *b* exposes the interfacial surface and displaces the [2Fe-2S] center so that no possibility of contact with the occupant of the binding pocket could occur. The position seen in the native chicken structure is 4.0 Å further from the heme of cyt c_1 than the position of closest approach seen in the beef $P6_522$ crystals (see Figure 2, top). The distance between the two positions of the [2Fe-2S] in the chicken structures is ∼16 Å and can be fitted by a simple rotation through 57°. The full range of movement is likely to be greater. We have suggested that the position seen in the native beef $P6_522$ crystals is the best representation of the configuration for reaction with cyt c_1 (*7*). The distance between the position of the [2Fe-2S] center in the chicken stigmatellin structure and in the native beef $P6_522$ structure gives a total displacement of ∼22 Å. This movement would require a rotation through ∼63°, combined with a small linear displacement, in a screw movement. The movement allows electron transfer over a distance of ∼32 Å, as given by the distance between the nearest O atom of stigmatellin and the Fe atom of heme c_1. The tertiary configuration within the head domain is, within the 3−3.5 Å resolution of the structures, unchanged between the different positions. The anchoring tail also remains fixed. The main action is confined to a short hinge region between residues 63 and 73, where a helical configuration in the native structure extends to a chain in the stigmatellin structure (see inset in Figure 2, top, and also Figure 5).

Role of ISP Movement in the Mechanism of the Bifurcated Reaction. It is generally assumed that oxidation of QH_2 involves transient production of a semiquinone (*10*−*14*, *40*), which is rapidly consumed in the second electron transfer to heme b_L. In the Q cycle, this mechanistic bifurcation is necessary for the overall energy-conserving function, since the electrogenic reactions, and consequently the H^+-pumping activity, depend on the electron transfer through the low-potential chain. The high efficiency of proton pumping reflects the high efficiency of the bifurcated reaction; indeed, under appropriate conditions the reaction can be driven in reverse by the proton gradient. We discuss the mechanism of the bifurcated reaction in detail in a separate paper (*23*) and summarize points pertinent to this paper below.

The reaction at the Q_o site proceeds from a reaction complex between quinol and oxidized ISP, but is limited by a high activation barrier, so that the products (semiquinone and the reduced [2Fe-2S] cluster in the free ISP head) are formed at the limiting rate. Because the equilibrium constant for formation of semiquinone is very small (*14*), the reaction proceeds only on removal of products. These do not accumulate even when removal is blocked (*14*, *40*). These properties of the reaction complex are critical to the bifurcation of the reaction.

The spatial separation between the two reaction interfaces of the ISP ensures that the [2Fe-2S] center is at a distance from cyt c_1 when it accepts an electron from quinol. The domain movement has to occur before the [2Fe-2S] can donate the electron to cyt c_1.

The formation of the reaction complex requires the intimate docking of ISP^{ox} on cyt *b*. The structure of the enzyme in the presence of stigmatellin, which we discuss in greater detail below, provides important clues as to the nature of the docking configuration.

Stigmatellin and UHDBT Binding. For UHDBT, stigmatellin, and quinone, interaction with the ISP induces a change in the EPR spectrum (*27*−*36*). The change is on the reduced form of the ISP, which must therefore be bound at the cyt *b* interface, with the [2Fe-2S] cluster close to the Q_o site, as is observed in the stigmatellin structure. The interaction with stigmatellin changes the E_m value of the [2Fe-2S] center from 290 to ∼540 mV, indicating a strong ligation of the reduced form. It seems likely that, in the crystals, either stigmatellin induces a reduction of the [2Fe-2S] center or the center is already reduced. In the structure shown in Figure 2 and Figure 3B (bottom), stigmatellin forms a H-bond to the Nϵ2 of His-161 and a ligand to the [2Fe-2S] of ISP through Nδ1 (*3*). From the change in E_m induced in the ISP, stigmatellin has a differential binding free energy between reduced and oxidized forms of ∼24 kJ/mol. The liganding force is clearly sufficient to constrain the ISP with relatively high occupancy at the cytochrome *b* interface. This constraint would restrict movement of the ISP, preventing electron transfer from the reduced [2Fe-2S] center to cytochrome c_1, since it would prevent the rotation of the mobile head to the ISP_C position from which the reaction with cyt c_1 is favored. A similar constraint through interaction of the ISP with UHDBT is expected. This would explain why in the presence of UHDBT the [2Fe-2S] center remained reduced under steady illumination, when the reaction center was sufficiently oxidized to favor oxidation of the center (*27*). We have estimated the occupancy of the ISP directly from the electron densities in crystals with stigmatellin or UHDBT, and confirmed these expectations (*22*). In the stigmatellin-containing crystals, the occupancy of the ISP_B position is 100% (within error), and in the UHDBT-containing crystals, ∼30%, reflecting the weaker differential binding of reduced ISP, compared with an occupancy of ∼10% in the native crystals. In the native and UHDBT-containing crystals, occupancy of the ISP_C position was ∼50% and ∼30%, respectively.

Stigmatellin Complex as a Model for the Reaction Complex. Crofts and Wang (*14*) showed that formation of a reaction complex of bound QH_2 preceded the activated step in quinol oxidation. Lancaster and Michel (*41*, *42*) have suggested, on the basis of modeling of stigmatellin at the Q_B site of the reaction center of *Rhodopseudomons viridis*, that stigmatellin mimics an intermediate of the reaction pathway, possibly a bound QH^- or $QH^\bullet$ intermediate. If we adopt this suggestion for the Q_o site case, the stigmatellin complex with the reduced [2Fe-2S] center might mimic the complex between quinol and the oxidized ISP:

$$E{\cdot}b_L{\cdot}QH_2 + [2Fe\text{-}2S]^{ox} \rightarrow \{E{\cdot}b_L{\cdot}QH_2{-}[2Fe\text{-}2S]^{ox}\} \rightarrow E{\cdot}b_L{\cdot}Q^{\bullet -} + H{\cdot}[2Fe\text{-}2S]^{red} + H^+$$

Link (*39*) had suggested that stigmatellin might mimic a reaction complex between semiquinone and the reduced ISP ($QH^{\bullet}-[2Fe\text{-}2S]^{red}$). He pointed out that such a complex might favor the binding of the reduced over the oxidized form of the ISP and so raise the E_m value of the [2Fe-2S] center. If the effect were of the same magnitude as the liganding by inhibitors, the potential might be raised enough so that the ISP could no longer act as an effective donor to cyt c_1, and the ISP would remain in this liganded state until electron transfer from the $QH^{\bullet}$ to cyt b_L had occurred, thus ensuring that the decoupling reaction between the semiquinone and the ISP^{ox} (the paradox discussed above) would not occur. In this mechanism, the rate-limiting step would be the second electron transfer. Kim et al. (*9*) have also discussed an essentially similar model in which transfer of both electrons would occur from the reaction complex with ISP. For mechanisms of this sort, it might be more appropriate to represent the reaction intermediate as a mixture of states, $QH_2-[2Fe\text{-}2S]^{ox}$ and $QH^{\bullet}-H^{\bullet}[2Fe\text{-}2S]^{red}$.

The movement of the ISP provides a new perspective on these aspects of mechanism. For any mechanism in which dissociation of the reaction complex is the rate-limiting step and shows a high activation barrier (*14*, *22*, *39*), the reaction complex, either between quinol and the oxidized subunit in the ISP_B position (*22*) or between semiquinone and reduced ISP (*9*, *39*), would also separate the ISP from its electron acceptor. Because of the high activation barrier, the reaction would proceed to the right only on removal of the semiquinone by oxidation through cyt b_L. Dissociation to product would lead to liberation of the reduced ISP from the cyt *b* interface, rapid diffusion to the cyt c_1 interface, and electron transfer through both chains at the limiting rate. Since either type of complex would fulfill this function, there is no need to invoke special redox properties for the complex as suggested by Link (*39*). We discuss the further processing of the semiquinone in greater detail in a separate paper (*23*).

Although the earlier work by Rieske et al. (*16*−*18*) had suggested that antimycin destabilized the ISP , subsequent work characterizing the mechanism has shown clearly that the reactions of the Rieske subunit are associated with the Q_o site, rather than the Q_i site at which antimycin binds, so this effect of antimycin was somewhat paradoxical. The structure around the Q_o site in the presence of stigmatellin is not markedly affected by the additional presence of antimycin (*7*), and it therefore seems likely that antimycin had an indirect effect in these early experiments. Possibly, addition of antimycin led to reduction of the quinone pool, which was the direct causative effect. We have shown using fluorescence resonance energy transfer that reduction of the quinone pool leads to movement of ISP away from cyt *b*, in line with this suggestion (*43*).

Mobility and Binding of the ISP: Complementary Functional Aspects. The crystallographic work has identified three main positions for the ISP. It might be supposed that these represent preferred binding locations. However, the operational parameters suggest a more dynamic state.

(1) Rapid movement from one configuration to the other requires that, in the partial reactions that require movement, the mobile domain should not be constrained by strong binding forces.

(2) As discussed above, in the stigmatellin structures, the ISP is held by liganding forces at the cyt *b* interface. No such binding was seen in our crystals containing either MOA inhibitors or myxothiazole since with these inhibitors, most of the ISP was in the same position as in the native crystals. Moreover, when antimycin was present with stigmatellin, binding of the former did not impede the ISP displacement due to the latter (*7*). With UHDBT, both ISP_B and ISP_C positions were occupied equally. It is clear that the ISP can move between the two positions in the chicken complex, but the movement to the ISP_B position is induced by interaction with inhibitors occupying the distal lobe of the Q_o site, to an extent depending on the binding energy associated with the change in E_m value. In contrast, in the work of Xia et al. (*6*), the [2Fe-2S] center was close to cyt *b* in all their structures. The differences between the structures of Xia et al. (*6*), and the positions in native or myxothiazole-containing structures from our own work (*7*), might reflect more subtle effects, perhaps in crystal packing forces, relative quinone content, or redox status. We have analyzed the protein electron densities in order to estimate occupancies of the ISP in both positions and concluded that, except for complexes with the site occupant, the association constants for the oxidized ISP are all relatively weak, suggesting that the mobile head is not tightly constrained by any protein interactions (*22*). In support of this, Kim et al. (*9*) have also reported changes in occupancy that accompany binding of different inhibitors. In their case, UHDBT or stigmatellin increased the density due to the FeS -cluster, and MOA-stilbene induced a loss of most of the density for the position close to cyt *b* where it is found in the structures of Xia et al. (*6*).

(3) Iwata et al. (*8*) have shown a third position for the ISP head in their $P6_5$ crystals, between the two positions in our chicken crystals, in which the ISP had a somewhat different configuration. The difference from the soluble fragment involved a displacement of the cluster-binding domain by a few angstroms and the breaking of a number of H-bonds. This configuration was found in only one monomer and appears to be associated with crystal contacts for the ISP head. Coordinates for the second ISP head were not included in the published structure, and the authors indicated that the structure was disordered, with partial occupancy of at least two positions. Although the authors suggest a significant physiological role for the new configuration, it seems unlikely that the two ISP heads are in different physiological states, and it is difficult to support the argument that the fixed head is the mechanistically relevant one.

These observations suggests a scenario in which the ISP is able to move relatively freely between the positions seen in the different crystals. In the ISP_C condition, a set of weak binding forces constrains the protein to a position close to cyt c_1 from which it can react rapidly with the cyt c_1 heme. In the ISP_B condition, a different set of weak forces constrains the system so that occupancy of the cyt *b* binding domain is higher, to favor formation of the reaction complex with quinol. The low Fe density for the cluster seen in the data of both the Zhang et al. (*7*) and Kim et al. (*9*) suggests that a significant fraction of the ISP head is not bound in either position, and this is confirmed by more detailed analysis of protein occupancy (*22*). The different positions may be thought of as mapping the trajectory of the displacement between the positions near cyt *b* and near cyt c_1. The

only strong associations indicated in the crystals are those seen when stigmatellin or UHDBT is present. If these mimic the reaction complex, that also would represent a strong association.

Interaction of Quinone with the ISP. Interactions between quinone at the Q_o site and the reduced ISP have been explored through the $g_x = 1.800$ band of the EPR spectrum of the [2Fe-2S] center. Earlier work showed effects of the redox state of the quinone pool, or of depletion by extraction, on the $g_x = 1.800$ band of mitochondria, chromatophores, or the isolated complex (*44*−*46*). Ding et al. (*33*−*35*), using wild-type and mutant strains from *Rb. capsulatus*, have investigated the effects of quantitative extraction of ubiquinone and concluded that different spectral changes can be detected at different local concentrations of the quinone pool. They suggested that these reflect two different populations of bound quinone at the Q_o site, called Q_{os} and Q_{ow} for strongly and weakly binding species, with both sites binding Q and QH_2 with equal affinity (i.e., with no change in E_m with respect to the pool).

Brandt (*47*, *48*) and Brandt and Okun (*49*) have also adopted a double-occupancy model. They have suggested a proton-gated charge-transfer mechanism to account for the paradox of the bifurcated reaction at the Q_o site.

We have previously discussed some difficulties with the double occupancy model (*15*, *50*) and have preferred a single-occupancy model in the companion paper (*23*), but we note here that the $g_x = 1.800$ EPR signal is found only when quinone is present in the pool and the [2Fe-2S] center is reduced. We have suggested that the $g_x = 1.800$ signal reflects the close interaction between quinone bound at the end of the pocket distal from heme b_L and the reduced ISP docked at the interface on cytochrome *b* (*15*, *23*). This simple interpretation allows us to use the $g_x = 1.800$ signal as diagnostic of this interaction and provides a tool to explore the effects of mutation.

Mutations at the ISP Docking Interface. Two binding processes on cyt *b* contribute to formation of the reaction complex that precedes the quinol oxidation reaction, one involving a binding interface for the ISP, and a second involving binding of the quinol. Since the residues contributing to the two binding domains are not a common set, mutations that affect function might be expected at either of these interfaces. The extensive set of data on occupancy of the site in different mutant strains, as reflected in the $g_x = 1.800$ EPR signal of the [2Fe-2S] center, provides important clues to mechanism (*33*−*35*, *50*; B. Barquera, A. R. Crofts, R. Gennis, P. L. Dutton, and H. Ding, unpublished results). We can distinguish three different locations for mutations, which correspond to three distinct phenotypes; mutations at the ISP docking interface; mutations around the distal lobe of the binding pocket, where the stigmatellin ring binds; and mutations around the proximal lobe, where the pharmacophore groups of myxothiazole and MOA-stilbene are observed. Mutations in the first group are primarily of concern in this paper.

Analysis of the native and stigmatellin structures shows that several residues at which effects of mutation have been studied lie at the interface between cyt *b* and ISP. Residues on cyt *b* with contacts to the ISP in the stigmatellin-containing structure are at Thr-145, Asn-149, Pro-262, Ile-269, Tyr-279, Leu-282, and Lys-288; other mutational sites within 5 Å of the ISP head domain are Gly-143, Thr-148, and Gly-191 (see Figure 4A). Mutations at a number of these sites (G143, T145, T148, I269, L282, and K288) slow or block electron transfer and prevent formation of the $g_x = 1.800$ signal. The effects of mutation can be understood in terms of an interference with the docking and can be explained in the context of the movement of the ISP suggested here. It seems likely that they interfere with the access of the ISP to the occupant of the Q_o pocket, and prevent the formation of a complex between the quinone and the ISP^{red} that gives rise to the $g_x = 1.800$ signal. These strains all have an inhibited rate of electron transfer at the site, though some are able to turn over at a rate sufficient to allow photosynthetic growth. We suggest that the rate of quinol oxidation at the Q_o site will depend on the probability of formation of the reaction complex between QH_2 and ISP^{ox} and that the reduced rate observed in these strains reflects the same impediment to access as that leading to loss of the $g_x = 1.800$ signal.

In addition to these mutations in cyt *b*, changes in the ISP that modify residues at the docking interface also interfere with function. Several mutations in the set generated by Gatti et al. (*51*) can now be seen to be at the interface. Most changes to the highly conserved residues close to the [2Fe-2S] center led to loss of function or failure of assembly (*52*−*57*), but a change at Gly-143 to aspartate, surprisingly, was functional. Van Doren et al. (*54*) constructed the equivalent mutation in *Rb. sphaeroides*, which, as in the mitochondrial complex (*51*), was functional, had a reduced rate of quinol oxidation, and had no $g_x = 1.800$ band. We have recently constructed a more extensive set of mutations at this residue (R. Kuras, M. Guergova-Kuras, A. R. Crofts, unpublished work) in which Ser, Asn, Tyr, Glu, and Ile showed activity, but Cys, His, Lys, and Pro did not. Homology models of the mutant subunits showed van der Waals contact with cyt *b* that correlated with loss of function. Liebl et al. (*55*) have explored a set of changes at residues equivalent to Thr-140 and Leu-142 to R, D, H, and G. In all three sets, change led to reduced rates of electron transfer or loss of function, even though mutant strains assembled an ISP with an identifiable [2Fe-2S] center. In the latter studies, loss of function for all Leu-142 mutants was associated with a loss or modification of the $g_x = 1.800$ signal. It seems possible, therefore, that these changes interfered with docking, and inspection of the structure shows that Leu-142 and Gly-143 are at the interfacial surface, with the leucine in close contact with cyt *b*, but the Cα H of glycine facing a small unoccupied volume (Figure 4B). Brasseur et al. (*56*) noted second-site suppressor strains that restored activity to lethal mutations at Leu-142 in which the modified residue was distant in the tertiary structure and close to the cleavage site in the structure of Iwata et al. (*3*). They speculated that these might indicate an involvement of this region in the correct orientation of the cluster. Mutations in yeast (*58*) or *Paracoccus denitrificans* (*59*) at the residue equivalent to conserved Tyr-165 gave rise to an inhibited electron transfer, but through a change in E_m for the cluster. Since the tyrosine is buried, the dependence of rate on free-energy change demonstrated in these experiments suggests a separate effect.

Other mutations that affect function at the site are deeper in the quinone-binding pocket, and are discussed in a separate paper (*23*).

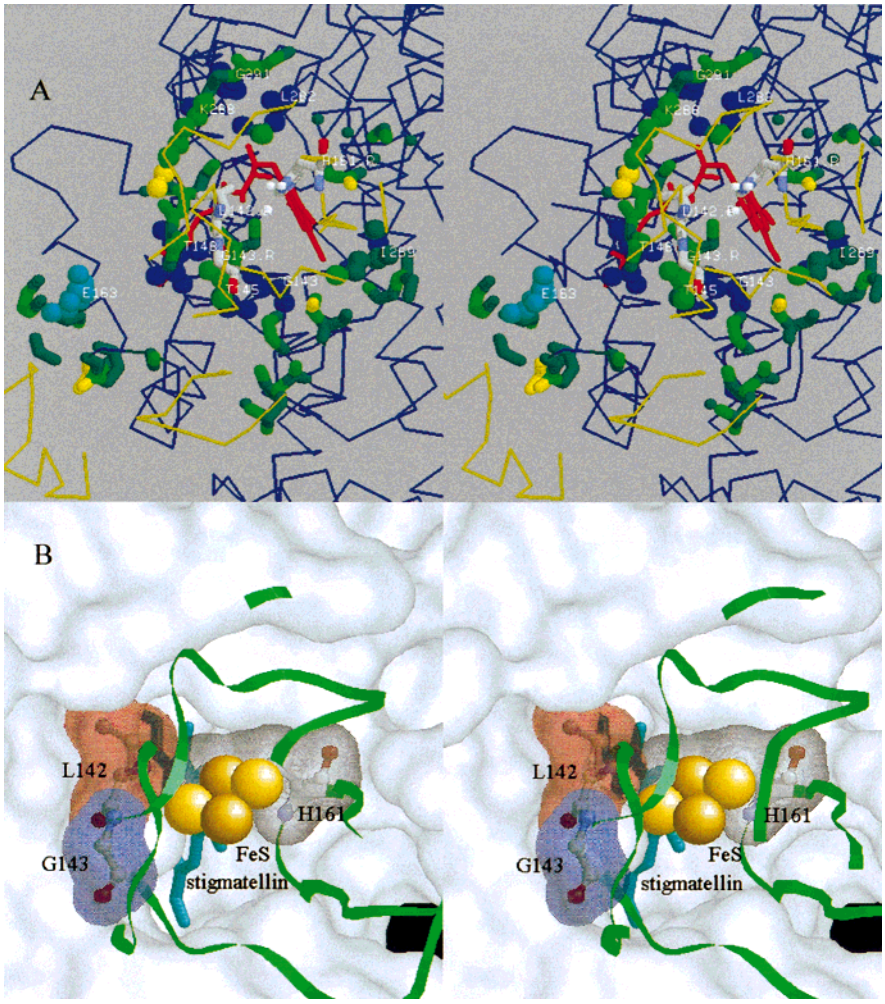

FIGURE 4: Residues at the interface of cyt *b* with ISP. (A) Cytochrome *b* and ISP subunits are shown as blue and green backbone structures, respectively. Atoms in cytochrome *b* that are close to the ISP head are shown as stick models colored blue (>5 Å), dark green (within 5 Å), green (within 4 Å), or yellow (within 3 Å). Residues at which mutation lowers or eliminates the $g_x = 1.800$ signal are emphasized as ball-and-stick models, and labeled at their Cα atoms. The cyan residue is Glu-163, the putative DCCD-binding residue, also within 5 Å of the ISP tail, seen as a backbone structure in the lower left corner. Stigmatellin is shown as a red wire-frame model, the [2Fe-2S] center is shown as small white spheres, and Leu-142, Gly-143, and His-161 of the ISP are shown as stick models colored CPK. (B) Docking of ISP against cyt *b* in the stigmatellin-containing structure, showing the tight packing of Leu-142. The surface of cyt *b* is shown in white, viewed from the ISP docking interface. The ISP is represented as a ribbon (green) with Leu-142, Gly-143, and His-161 as ball-and-stick models enclosed in their transparent surfaces (colored red, blue, and gray, respectively). The [2Fe-2S] cluster is shown as CPK-colored spheres. Stigmatellin is shown as a stick model in cyan. These panels are presented as a stereopair for crossed-eye viewing.

Anchoring of the ISP: a Role for the Dimer. The anchoring N-terminal tail of the ISP is locked in a tight vise provided by residues from both cyt *b* monomers, which interact with the ISP at residues 59−64 (Figure 5A). In one monomer (left), with which the tail interacts, residues 55 and 74−76 from the turn between the ab helix and helix B contribute one face of the vise. In the other monomer (right), with which the head interacts, residues 163 and 165−169 from the cd2 helix and 178 from the N-terminal end of helix D contribute the other face of the vise. Additional constraints on motion of the anchor are provided by a clamping of the ISP transmembrane helix between the membrane helix of cytochrome c_1 (on the inside) and the membrane helix of subunit X (on the outside) and by contacts with subunit VII and with subunit I on the matrix side of the complex. Clearly these interactions involve the dimeric structure, and are of importance in positioning the ISP head in an orientation appropriate for its exploration of the reaction domain.

The anchoring tail of the ISP contains two amphipathic sections. The section between residues 46 and 65, previously postulated to be a surface helix (*60*), is strongly amphipathic, with polar residues forming one side of the helix. The apolar face lines the cavity through which the lipid phase gains access to the quinone processing sites (*6*) (Figure 5B). The polar face interacts with polar residues in the vise, but is also exposed to the surface between residues 52 and 63 to create an environment in which the polarity is not compensated by a complementary protein interface. As part of this exposed face, Lys-52 interacts with Glu-32 of subunit X. This polar surface extends into the lipid phase almost halfway across the membrane from the P phase. Possibly this face interacts with the polar lipid headgroups. The remainder of the helix in the transmembrane region (residues 34−45) is more hydrophobic, but also amphipathic, with the polar face rotated around the helical axis compared to the C-terminal end. This more N-terminal polar face is also exposed to the surface and brings a polar interface partway across the lipid phase from the other side (the N-side).

From profiles for hydrophobic moment and hydropathy and from helical wheel plots, it is apparent that these

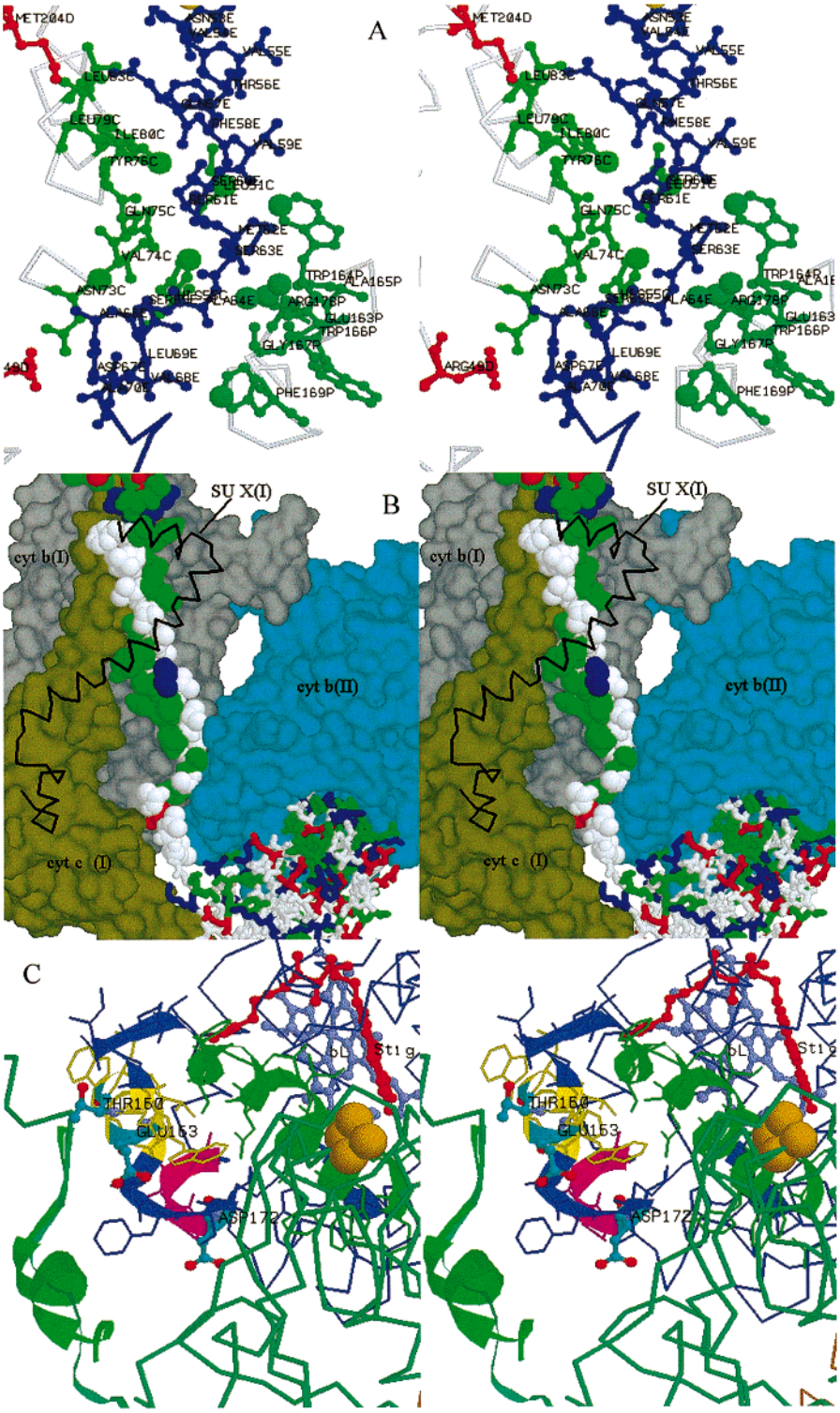

FIGURE 5: Anchor, hinge, and vise regions of the ISP and cytochrome *b*. (A) Residues contributing to the vise. The ISP tail (chain E) is shown as a blue ball-and-stick structure. Residues with atoms within 4.0 Å in other chains are also shown as ball-and-stick models. Cyt *b*, pale blue-green (chain P) or green (chain C); cyt c_1, red (chain D). Residues within 3.25 Å are highlighted as enlarged spheres. Residues are labeled at their Cα atoms. The structure is that of the native dimeric complex. (B) Anchoring region of the N-terminal segment of the ISP, showing the amphipathic structure. This is a stereoview of components in the dimeric structure containing stigmatellin. The N-terminal 69 residues of the ISP are shown as space-filling spheres, colored according to hydropathy as follows: Leu, Val, Ile, Ala, Met, Phe, and Trp, white; Asn, Gln, Cys, Pro, Tyr, Gly, Ser, and Thr, green; His, Arg, and Lys, blue; Asp and Glu, red. The C-terminal section (after residue 70) is shown as a stick model, similarly colored. The subunits interacting with the anchor in the membrane are shown by their surfaces, as follows: cyt *b* (monomer I), gray; cyt *b* (monomer II), cyan; cyt c_1 (monomer 1), brown. Subunit X of monomer I is shown as a black backbone, so as not to obscure the ISP tail. (C) Residues at which DCCD binds in different species, and the hinge of the ISP. Cyt *b* is shown as a blue backbone, except for the cd loop, which is represented by a Richardson cartoon. The cd1 helix is colored green (right of figure); cd2 helix, yellow; D helix, magenta; connecting loops, blue. The DCCD binding groups are shown as ball-and-stick models, with C atoms in cyan. Other residues contributing to the span are shown as wire-frame models. The ISP hinge region (left) is shown as a Richardson cartoon of the native configuration (green helical structure), and the stigmatellin-induced configuration is shown as a green-blue coil. The rest of the ISP is shown in the stigmatellin-induced configuration as a green-blue backbone, with the [2Fe-2S] center as a space-filling model in CPK colors. Stigmatellin (red) and heme b_L (mauve) are shown as ball-and-stick models. (These panels are presented as stereopairs for crossed-eye viewing.)

amphipathic and hydrophobic features are conserved across the bacterial/mitochondrial boundaries. The anchoring tail in b_6f complexes shows a similar structural theme, but the amphipathic span precedes the hydrophobic span in the sequence, instead of the other way around. The amphipathic nature of the anchor and the polar interactions provide an explanation for the ease with which the ISP is dissociated from the complex by treatments that include high ionic strength or chaotropic agents (*16*−*21, 52, 53*). The striking conservation of the amphipathic features of the ISP anchor across taxon boundaries suggests that these structures reflect a functional importance. The length of the transmembrane span (made possible by the 45° tilt), the amphipathic nature, and the polar interactions involved might provide a more rigid anchoring than would be the case for a hydrophobic membrane helix. In view of the fact that no differences in the anchor are seen between the configurations in the different structures, the relative ease with which the ISP is detached from the complex probably does not reflect a weak attachment under physiological conditions. Indeed, it is difficult to imagine a physiological role for a weak attachment.

Modifications of the Hinge and Vise that Affect Turnover of the bc_1 Complex. Several lines of evidence have suggested that modification of the vise region or hinge might affect reactions at the Q_o site. The second-site revertants from Daldal's work discussed above, which suppress the pho$^-$ phenotype of lethal mutants at the residue equivalent to ISP L142 in *Rb. capsulatus*, are in the hinge region of the ISP (equivalent to residues 68 and 70 in the structure of Iwata et al.) (*55, 56*). Possibly they have their effect by correcting the misaligned docking in the mutants. In light of the structure, other examples of suppressor effects for mutations near the Q_o site by mutations in the vise or hinge region can be identified from those catalogued by Brasseur et al. (*36*). These include G137E/F151L (in yeast), T163F/G182S (in *Rb. capsulatus*, equivalent to T148 and G167 in chicken), and also T163F/ISP-A46T (in *Rb. capsulatus*, equivalent to T148 and ISP D70 in chicken), recently described in greater detail (*57*).

In mitochondrial complexes, DCCD blocks proton pumping by the bc_1 (or b_6f) complex, but not electron flow (the decoupling effect), by binding to an acidic residue in the cd2 loop of the cyt *b* subunit (*61*). Brandt and Trumpower (*13*) have suggested that this decoupling may involve access to a cryptic H^+ channel at the Q_o site. In yeast, Asp-160 is the binding site for DCCD, but this residue is not conserved, and Wang et al. (*61*) have suggested that Glu-163 may also be a target, for example, in the bovine complex and in the b_6f-complex. *Rb. sphaeroides* has neither of these acidic residues in the cd2 helix and is less sensitive to DCCD at concentrations leading to inhibition in these other systems (unpublished observations). Wang et al. (*62*) have recently shown that, at higher concentrations, Asp-187 in the turn linking the cd2 and D helices (equivalent to Asp-172 in yeast) is labeled by DCCD and has a decoupling effect. Earlier results from Takamiya (*63*) had shown inhibition of electron flow, rapid H^+ uptake, and electrogenic processes of the bc_1 complex, all with a similar titration and no uncoupling. He concluded that DCCD was an electron-transfer inhibitor. The sequences for cyt *b* in the labeled region are shown aligned below. The residues in boldface italic type are those shown (or thought) to be labeled by DCCD. The structure of the span in the chicken complex is shown above the alignment (C, coil; T, turn; H, helix), and the architectural role is shown below, encoded as follows: s, structural within cyt *b*; v, the vise that locks the ISP tail; i, interface with the mobile head of the ISP; x, cross-interaction with cyt *b* of the other monomer; e, exposed to aqueous phase; b, buried in lipid phase.

```
                    CTTTTHHHHHHHTTTTTTTHHHHHHHH

                          160          172

                         {-cd2-}        [=====D=-----
Yeast               IPFVGN***D***IV***S***WLWGGFSV***S***NPTIQRFF----

Chicken             IPYIGH***T***LV***E***WAWGGFSV***D***NPTLTRFF----

Bovine              IPYIGT***N***LV***E***WIWGGFSV***D***KATLTRFF----

Spinach b6/f        IPVIGS***P***LV***E***LLRGSASV***G***QSTLTRFY----

*R. sphaeroides*    IPGIGH***S***IQ***T***WLLGGPAV***D***NATLNRFF----

                    ssbssbebsevvbvvviseexssxvsx
```

The structure of the chicken complex shows that all three residues lie in the cd loop, with T160 and E163 in the cd2 helix and D172 in a coil immediately before helix D. All three side chains are exposed at the P-phase surface [the intermembrane (periplasmic) surface] of cyt *b*, likely at the level where the polar phospholipid headgroups would interface when the complex is in the membrane. All three residues are also close to the interface between cyt *b* and the ISP in the region of the vise (in cyt *b*) and hinge (in ISP) (Figure 5C), where the ISP anchor is bound between the two cyt *b* subunits of the complex. They are also close to, but do not impinge directly on, the interface between cyt *b* monomers. They are relatively distant from the Q_o site (∼19 Å from Cα of each residue to the nearest carbonyl of stigmatellin), and none is in contact with the head of the ISP in either configuration.

If binding to the residues in the cd2 helix is the only effect of DCCD, the inhibitory effect is difficult to explain. It seems possible that, after reaction, the additional bulk of the DCCD adduct distorts the structure so as to interfere with anchoring or movement of the ISP. Similarly, the remote second-site revertants might have their effects by subtle structural changes. These effects of remote change on catalysis at the Q_o site could have a number of different mechanisms.

(1) Since the DCCD-binding residues are close to the vise, the presence of the DCCD adduct might interfere with the anchoring. We have noted above the peculiar amphipathic structure of the anchor and the polarity it brings into the membrane phase. The polarity of the exposed surfaces raises the possibility of their hydration. If the packing of this helix were perturbed, further hydration might occur, with formation of a H^+-conducting channel. This could provide a proton leak, along the lines suggested by Brandt and Trumpower (*13*). Although no static leak is seen after DCCD treatment, one could speculate that a leak might be dynamically linked to turnover of the Q_o site. Brandt and Trumpower suggested that the binding of DCCD might perturb proton access to the Q_o site. However, the DCCD-reactive residues are all 18−20 Å away from the Q_o site and are unlikely to take part in proton processing at the site (*13*).

(2) Another possibility is that distortion of the structure might be transmitted indirectly to the Q_o site through the cd1 helix. Since the binding of the Q_o occupant involves a displacement of the cd1 helix, any change that hindered this displacement would have consequences for the mechanism. For example, such a change might restrict binding of semiquinone in the proximal domain or destabilize the reaction complex in the distal domain or both. If the semiquinone were unable to reduce heme b_L, then the bifurcated reaction would not occur, and the electrogenic electron transfer across the membrane essential for net H^+ transfer would be prevented. To account for the decoupling, this inhibitory effect would also have to allow forward electron transfer from semiquinone to the [2Fe-2S] center, so that the second electron could follow the first down the high-potential chain. This might occur only under static head conditions when electrons are backed up in the low-potential chain by back pressure from the proton gradient.

(3) The hinge of the ISP between residues 65−72 undergoes a substantial conformational change (as shown in Figure 2, top, and Figure 5C by the cartoon structure of residues 63−73 of the ISP in both ISP_B and ISP_C configurations), leading to changes in contacts with residues in the cd span in the region of cyt *b* forming the vise. From the mutational studies (*55*−*57*), relatively modest changes in the hinge ameliorate effects of mutation at the interface, so one might anticipate that the DCCD adduct would interfere with the hinge and perturb the "swing" of the head and the accuracy of the docking. This might impede formation of the reaction complex or destabilize it, favoring the decoupled reaction.

It seems unlikely that the cryptic H^+-channel invoked in possibility 1 would form part of the physiological reaction, and it certainly does not fit naturally into the conventional mechanistic discussions of the Q cycle. The situation of the anchor in the structure is far removed from the mechanistic action, and it is difficult to imagine how any aspect of the electron transfer process could be directly coupled to changes in activity of protons in the putative channel.

Other pathways for coupling an effect of DCCD binding to the proton processing of the Q cycle seem implausible. The side chains from both the ISP and cyt *b* contributing to the vise region are predominantly polar, and they form part of the polar P-phase interface, in direct contact with the aqueous phase. Their protonic contact with the Q_o site would therefore be via the aqueous phase. There are no obvious channels of polarity connecting the vise region more directly to either the Q_o site or the binding pocket for heme b_L. At the level of the dimeric complex, a cleft from the N-phase side between the two monomers appears to be insulated from the polarity at the P-phase interface by a band of hydrophobic side chains that would preclude participation in a H^+ conduction channel. Furthermore, the residues lining the cleft are predominantly hydrophobic, so it seems more likely that it is filled with lipid.

Movement of the ISP Represents a Novel Electron-Transfer Mechanism. The structures have revealed a novel mechanism for electron transfer. The 16−22 Å movement of the tethered head between two reaction interfaces allows for a rapid reaction over a substantial distance (∼32 Å between stigmatellin O and cyt c_1 Fe). In solid-state systems, equivalent rates are achieved by a fixed intermediate redox carrier (*64*). Although the main evolutionary advantage of the more flexible arrangement probably pertains to the peculiar mechanism of the bifurcated reaction (*22, 23*), the tethered head mechanism might provide other useful options. By constraining the local diffusional domain, the mechanism avoids the entropic loss of free diffusion and the slower rate of the second-order reaction resulting from dilution in a larger volume. Such properties might be expected to have a selective advantage and to be used in other electron-transfer chains.

In *Rb. capsulatus*, Myllykallio et al. (*65, 66*) have demonstrated that, in addition to cyt c_2, a membrane-bound cyt c_y transfers electrons between the bc_1 complex and the reaction center. From the sequence, this cytochrome appears to have a conventional cyt *c* head attached to a single transmembrane helical anchor by a linking chain. Although cyt c_y allows growth of *Rb. capsulatus* strains deleted in cyt c_2, the kinetics of reduction of the reaction center after photoactivation show that only a fraction (20−30%) of the bc_1 complexes visited by the mobile cyt c_2 in wild type are within the reaction domain seen by cyt c_y in a cyt c_2 deletion strain. In *Rb. sphaeroides*, which has a similar component, the membrane-bound cytochrome cannot replace cyt c_2 in the cyclic chain. When the native cyt c_y of *Rb. capsulatus* was replaced by the cyt c_y from *Rb. sphaeroides*, which has a shorter linker, no electron transfer between the bc_1 complex and reaction center was seen. However, both cyt c_y proteins could catalyze the electron transfer between the bc_1 complex and cytochrome oxidase. Myllykallio et al. (*66*) suggested that the important difference was that of the length of the linker connecting the cyt *c* head with the anchor. From the structures of the bc_1 complex and cytochrome oxidase dimers and from a model of the reaction center with LH1 in position (*67, 68*), the closest approach between reaction partners can be estimated. The main difference between the electron transfer from the bc_1 complex to the reaction center (∼87 Å distance for nearest approach between donor and acceptor centers) and that to cytochrome oxidase (∼54 Å distance of closest approach) is the presence of a cylindrical barrier of the LH1 light-harvesting complex, which separates the reaction center protein from its neighbors in the membrane by an additional ∼23 Å. The *Rb. capsulatus* cyt c_y would have to span the large distance, suggesting a linker of at least 45 Å. It seems likely that cyt c_y is another example of a tethered electron-transferring head but with a wider reaction domain than the ISP. In the *Rb. capsulatus* protein, the range is sufficient to allow electron transfer to the reaction center, but the *Rb. sphaeroides* protein has a shorter linker that limits the range.

A second example is the reaction catalyzed by a cyt c_{551} in *Chlorobium* species. The cytochrome appears to be tethered to a three-helix membrane anchor by a long linker (*69*) and acts as donor to the PS I-like reaction center and also as the electron carrier between the reaction center and a truncated bc_1 complex (*70*).

Although numerous examples of protein motion have been reported and analyzed in some detail (*71*), this is the first well-defined example of a simple electron transfer reaction involving a substantial domain movement. Other bioenergetic processes involve substantial conformational changes, most notably in the ATP synthase reaction, muscle contraction, microfilament walking, bacteriorhodopsin, the bacterial

flagella motor, and cilia beating. Other redox reactions with a notable domain movement are thioredoxin reductase and glutathione reductase (*72*), where a hinge motion is thought to bring either the NADPH binding site or the cysteine pair to a position for redox exchange with bound FAD.

ACKNOWLEDGMENT

We acknowledge helpful discussions with Drs. Fevzi Daldal, Les Dutton, Wolfgang Nitschke, and Thomas Link.

REFERENCES

1. Martinez, S. E., Huang, D., Szczepaniak, A., Cramer, W. A., and Smith, J. L. (1994) *Structure 2*, 95−105.
2. Berry, E. A., Huang, L.-s., Chi, Y., Zhang, Z., Malkin, R., and Fernandez-Velasco, J. G. (1997) Biophysical Society Annual Meeting, New Orleans, LA, March 1997, Abstract Tu-AM-L7.
3. Iwata, S., Saynovits, M., Link, T. A., and Michel, H. (1996) *Structure 4*, 567−579.
4. Carrell, C. J., Zhang, H. M., Cramer, W. A., and Smith, J. L. (1998) *Structure 5*, 1613−1625.
5. Yu, C.-A., Xia, J.-Z., Kachurin, A. M., Yu, L., Xia, D., Kim, H., and Deisenhofer, J. (1996) *Biochim. Biophys. Acta 1275*, 47−53.
6. Xia, D., Yu, C.-A., Kim, H., Xia, J.-Z., Kachurin, A. M., Zhang, L., Yu, L., and Deisenhofer, J. (1997) *Science 277*, 60−66.
7. Zhang, Z., Huang, L., Shulmeister, V. M., Chi, Y.-I., Kim, K. K., Hung, L.-W., Crofts, A. R., Berry, E. A., and Kim, S.-H. (1998) *Nature (London) 392*, 677−684.
8. Iwata, S., Lee, J. W., Okada, K., Lee, J. K., Iwata, M., Rasmussen, B., Link, T. A., Ramaswamy, S., and Jap, B. K. (1998) *Science 281*, 64−71.
9. Kim, H., Xia, D., Yu, C.-A., Xia, J.-Z., Kachurin, A. M., Zhang, L., Yu, L. and Deisenhofer, J. (1998) *Proc. Natl. Acad. Sci. U.S.A. 95*, 8026−8033.
10. Mitchell, P. (1976) *J. Theor. Biol. 62*, 327−367.
11. Crofts, A. R., Meinhardt, S. W., Jones, K. R., and Snozzi, M. (1983) *Biochim. Biophys. Acta 723*, 202−218.
12. Crofts, A. R. (1985) in *The Enzymes of Biological Membranes* (Martonosi, A. N., Ed.), Vol. 4, pp 347−382, Plenum, New York.
13. Brandt, U., and Trumpower, B. L. (1994) *CRC Crit. Rev. Biochem. 29*, 165−197.
14. Crofts, A. R., and Wang, Z. (1989) *Photosynth. Res. 22*, 69−87.
15. Crofts, A. R., Barquera, B., Gennis, R. B., Kuras, R., Guergova-Kuras, M., and Berry, E. A. (1999) in *The Phototrophic Prokaryotes* (Peschek, G. A., Loeffelhardt, W., and Schmetterer, G., Eds.) pp 229−239. Plenum, New York.
16. Rieske, J. S., MacLennan, D. H., and Coleman, R. (1964) *Biochem. Biophys. Res. Commun. 15*, 338−344.
17. Rieske, J. S., Baum, H., Stoner, C. D., and Lipton, S. H. J. (1967) *J. Biol. Chem. 242*, 4854−4866.
18. Rieske, J. S. (1976) *Biochim. Biophys. Acta 639*, 129−155.
19. Trumpower, B. L., and Edwards, C. A. (1979) *J. Biol. Chem. 254*, 8697−8706.
20. Breyton, C., de Vitry, C., and Popot, J. L. (1994) *J. Biol. Chem. 269*, 7597−602.
21. Weiss, H. (1987) *Curr. Top. Bioenerg. 15*, 67−96.
22. Crofts, A. R., Hong, S., Zhang, Z., and Berry, E. A. (1999) Physicochemical Aspects of the Movement of the Rieske iron sulfur protein during quinol oxidation by the bc_1 complex from mitochondria and photosynthetic bacteria, *Biochemistry 38*, 15827−15839.
23. Crofts, A. R., Barquera, B., Gennis, R. B., Kuras, R., Guergova-Kuras, M., and Berry, E. A. (1999) Mechanism of ubiquinol oxidation by the bc_1 complex: different domains of the quinol binding pocket and their role in mechanism and binding of inhibitors, *Biochemistry 38*, 15807−15826.
24. French, G. S. and Wilson, K. S. (1978) *Acta Crystallogr. A34*, 517.
25. Kleywegt, G. J. and Jones, T. A. (1997) *Methods Enzymol. 277*, 208−230, citing a personal communication of Bart Hazes (1995).
26. Crofts, A. R., Hacker, B., Barquera, B., Yun, C.-H., and Gennis, R. (1992) *Biochim. Biophys. Acta 1101*, 162−165.
27. Bowyer, J. R., Dutton, P. L., Prince, R. C., and Crofts, A. R. (1980) *Biochim. Biophys. Acta 592*, 445−460.
28. Meinhardt, S. W., and Crofts, A. R. (1982). *FEBS Lett. 149*, 217−222.
29. Link, T. A., Haase, U., Brandt, U., and von Jagow, G. (1993) *J. Bioenerg. Biomembr. 25*, 221−232.
30. Schägger, H., Brandt, U., Gencic, S., and von Jagow, G. (1995) *Methods Enzymol. 260*, 82−96.
31. von Jagow, G., and Link, T. A. (1986) *Methods Enzymol. 126*, 253−271.
32. Matsuura, K., Bowyer, J. R., Ohnishi, T., and Dutton, P. L. (1983) *J. Biol. Chem. 258*, 1571−1579.
33. Ding, H., Robertson, D. E., Daldal, F., and Dutton, P. L. (1992) *Biochemistry 31*, 3144−3158.
34. Ding, H., Moser, C. C., Robertson, D. E., Tokito, M. K., Daldal, F., and Dutton, P. L. (1995) *Biochemistry 34*, 15979−15996.
35. Ding, H., Daldal, F., and Dutton, P. L. (1995) *Biochemistry 34*, 15997−16003.
36. Brasseur, G., Sami Saribas, A., and Daldal, F. (1996) *Biochim. Biophys. Acta 1275*, 61−69.
37. Degli Esposti, M., De Vries, S., Crimi, M., Ghelli, A., Patarnello, T., and Meyer, A. (1993) *Biochim. Biophys. Acta 1143*, 243−271.
38. Robertson, D. E., Daldal, F., and Dutton, P. L. (1990) *Biochemistry 29*, 11249−11260.
39. Link, T. A. (1997) *FEBS Lett. 412*, 257−264.
40. Jünemann, S., Heathcote, P., and Rich, P. (1998) *J. Biol. Chem. 273*, 21603−21607.
41. Lancaster, C. R., and Michel, H. (1996) In *Reaction centers of photosynthetic bacteria. Structure and Dynamics* (Michel-Beyerle, M. E., ed.), International Workshop Feldafing III, pp 23−35, Springer-Verlag, Berlin.
42. Lancaster, C. R., and Michel, H. (1997) *Structure 5*, 1339−1359.
43. Crofts, A. R., Berry, E. A., Kuras, R., Guergova-Kuras, M., Hong, S., and Ugulava, N. (1998) in *Photosynthesis: Mechanisms and Effects* (Garab, G., Ed.). Vol. III, pp 1481−1486. Kluwer Academic Publishers, Dordrecht, The Netherlands.
44. De Vries, S., Albracht, S. P. J., and Leeuwerik, F. J. (1979) *Biochim. Biophys. Acta 546*, 316−333.
45. Ohnishi, T., Schagger, H., Meinhardt, S. W., LoBrutto, R., Link, T. A., and von Jagow, G. (1989) *J. Biol. Chem. 264*, 735−741.
46. de la Rosa, F. F., and Palmer, G. (1983) *FEBS Lett. 163*, 140−143.
47. Brandt, U. (1996) *Biochim. Biophys. Acta 1275*, 41−46.
48. Brandt, U. (1998) *Biochim. Biophys. Acta 1365*, 261−268.
49. Brandt, U., and Okun, J. G. (1997) *Biochemistry 36*, 11234−11240.
50. Crofts, A. R., Barquera, B., Bechmann, G., Guergova, M., Salcedo-Hernandez, R., Hacker, B., Hong, S., and Gennis, R. B. (1995) in *Photosynthesis: from light to biosphere* (Mathis, P., Ed.) Vol. II, pp 493−500, Kluwer Academic Publishers, Dordrecht, The Netherlands.
51. Gatti, D. L., Meinhardt, S. W., Ohnishi, T., and Tzagoloff, A. (1989) *J. Mol. Biol. 205*, 421−435.
52. Graham, L. A., Brandt, U., Sargent, J. S., and Trumpower, B. L. (1992) *J. Bioenegr. Biomembr. 25*, 245−257
53. Davidson, E., Ohinshi, T., Atta-Asafo-Adjei, E., and Daldal, F. (1992) *Biochemistry 31*, 3342−3351.
54. Van Doren, S. R., Gennis, R. B., Barquera, B., and Crofts, A. R. (1993) *Biochemistry 32*, 8083−8091.
55. Liebl, U., Sled, V., Brasseur, G., Ohnishi, T., and Daldal, F. (1997) *Biochemistry 36*, 11675−11684.

56. Brasseur, G., Sled, V., Liebl, U, Ohnishi, T., and Daldal, F. (1997) *Biochemistry 36*, 11685−11696.
57. Saribas, A. S., Valkova-Valchanova, M., Tokito, M., Zhang, Z., Berry, E. A., and Daldal, F. (1998) *Biochemistry 37*, 8105−8114.
58. Denke, E., Merbitzzahradnik, T., Hatzfeld, O. M., Snyder, C. H., Link, T. A., and Trumpower, B. L. (1998) Alteration of the midpoint potential of the Rieske iron−sulfur protein by changes of amino acids forming H-bonds to the iron−sulfur cluster, *J. Biol. Chem. 273*, 9085−9093.
59. Schröter, T., Hatzfeld, O. M., Gemeinhardt, S., Korn, M., Friedrich, T., Ludwig, B., and Link, T. (1998) Mutational analysis of residues forming hydrogen bonds in the Rieske [2Fe-2S] cluster of the cytochrome bc_1 complex of *Paracoccus denitrificans*, *Eur. J. Biochem. 255*, 100−106.
60. Gonzalez-Halphen, D., Vazquez-Acevedo, M., and Garcia-Ponce, B. (1991) *J. Biol. Chem. 266*, 3870−3876.
61. Wang, Y. D., Howton, M. M., and Beattie, D. S. (1995) *Biochemistry 34*, 7476−7482.
62. Wang, Y., Obungu, V., and Beattie, D. (1998) *Arch. Biochem. Biophys*. *352*, 193−198.
63. Takamiya, K.-I. (1983) *J. Biochem. (Tokyo) 94*, 1587−1593.
64. Moser, C. C., Page, C. C., Farid, R., and Dutton, P. L. (1995) Biological electron transfer, *J. Bioenerg. Biomembr*. *27*, 263−274.
65. Myllykallio, H., Jenney, F. E., Moomaw, C. R., Slaughter, C. A., and Daldal, F. (1997) *J. Bacteriol. 179*, 2623−2631.
66. Myllykallio, H., Drepper, F., Mathis, P., and Daldal, P. (1998) *Biochemistry 37*, 5501−551.
67. Cogdell, R. J., Fyfe, P. K., Barrett, S. J., Prince, S. M., Freer, A. A., Isaacs, N. W., Mcglynn, P., and Hunter, C. N. (1996) *Photosynth. Res. 48*, 55−63.
68. Hu, X. C., Ritz, T., Damjanovic, A., and Schulten, K. (1997) *J. Phys. Chem. B 101*, 3854−3871.
69. Okkels, J. S., Kjaer, B., Hansson, O., Svendsen, I., Moller, B. L., and Scheller, H. V. (1992) *J. Biol. Chem. 267*, 21139−21145.
70. Ohoka, H., Iwaki, M., and Itoh, S. (1997) *Biochemistry 36*, 9267−9272.
71. Gerstein, M., Lesk, A., and Chothia, C. (1994) *Biochemistry 33*, 6739−6749.
72. Waksman, G., Krishna, T. S., Williams, C. H., Jr., and Kuriyan, J. (1994) *J. Mol. Biol. 236*, 800−816.

BI990961U